LAWRENCE
LIVERMORE
NATIONAL
LABORATORY

UCRL-JRNL-204814

An Overview of High Energy Short Pulse Technology for Advanced Radiography of Laser Fusion Experiments

C. P. J Barty, M. Key, J. Britten, R. Beach, G. Beer, C. Brown, S. Bryan, J. Caird, T. Carlson, J. Crane, J. Dawson, A. C. Erlandson, D. Fittinghoff, M. Hermann, C. Hoaglan, A. Iyer, L. Jones, I. Jovanovic, A. Komashko, O. Landen, Z. Liao, W. Molander, A. Mitchell, E. Moses, N. Nielsen, H-H. Nguyen, J. Nissen, S. Payne, D. Pennington, L. Risinger, M. Rushford, K. Skulina, M. Spaeth, B. Stuart, G. Tietbohl, B. Wattellier

June 21, 2004

Nuclear Fusion Special Issue on IFSA 2003

AN OVERVIEW OF HIGH ENERGY SHORT PULSE TECHNOLOGY FOR ADVANCED RADIOGRAPHY OF LASER FUSION EXPERIMENTS

C. P. J. Barty, M. Key, J. Britten, R. Beach, G. Beer, C. Brown, S. Bryan, J. Caird, T. Carlson, J. Crane, J. Dawson, A. C. Erlandson, D. Fittinghoff, M. Hermann, C. Hoaglan,A. Iyer, L. Jones II, I. Jovanovic, A. Komashko, O. Landen, Z. Liao, W. Molander, S. Mitchell, E. Moses, N. Nielsen, H-H. Nguyen, J. Nissen, S. Payne, D. Pennington, L. Risinger, M. Rushford, K. Skulina, M. Spaeth, B. Stuart, G. Tietbohl and B. Wattellier

Lawrence Livermore National Laboratory, Mail Code L-490,
7000 East Avenue, Livermore, California 94550
Tel: 925-423-8486, FAX: 925-422-8297, e-mail barty1@llnl.gov

ABSTRACT

The technical challenges and motivations for high-energy, short-pulse generation with NIF-class, Nd:glass laser systems are reviewed. High energy short pulse generation (multi-kilojoule, picosecond pulses) will be possible via the adaptation of chirped pulse amplification laser techniques on the NIF. Development of meter-scale, high efficiency, high-damage-threshold final optics is a key technical challenge. In addition, deployment of HEPW pulses on NIF is constrained by existing laser infrastructure and requires new, compact compressor designs and short-pulse, fiber-based, seed-laser systems. The key motivations for high energy petawatt pulses on NIF is briefly outlined and includes high-energy, x-ray radiography, proton beam radiography, proton isochoric heating and tests of the fast ignitor concept for inertial confinement fusion

I. INTRODUCTION

The technique of chirped pulse amplification (CPA) [1] has allowed the generation petawatt peak power pulses [2] and focal intensities of order 10^{21} W/cm^2. [3] Petawatt laser pulses of ~500-J energy and a ~0.5-ps pulse duration are now or will be produced by a number of Nd:glass laser facilities around the world. High peak power pulses when focused to relativistic intensities (>10^{18} W/cm^2) allow longitudinal coupling of laser light to free electrons and have produced energetic, >MeV electrons, protons and x-rays. MeV particles and 10 keV to MeV photons could enable new, campaign-critical diagnostics to be deployed for NIF-scale experiments and could eventually allow the viability of full-scale fast ignition ICF to be tested on NIF. The energy of present petawatt laser systems, however, is insufficient to provide the necessary particle or photon flux for these missions and experiments on NIF. Estimates suggest that pulse energies that are 1 to 2 orders of magnitude (5 to 100 kJ) beyond the present state of the art (0.5 kJ) will be required.

With respect to radiography, full-scale NIF targets will present a significant radiographic challenge. Traditionally inertial confinement fusion experiments have been backlit with radiation from nanosecond, laser-produced plasmas. These plasmas emit radiation as a thermal blackbody. Low energy x-rays (4 to 10 keV) in the tail of the blackbody distribution are capable of penetrating the dense target to produce a nanosecond-time-scale, shadowgraph of a particular experiment. 100-ps time-resolution, detectors can be used to temporally resolve dynamics. While this technique is powerful and well established, it runs into severe limitations when considered for NIF-scale experiments. In general, NIF-scale targets will be of order 250 times larger volume than targets used in the Nova experimental campaign. Such targets are opaque to low-energy x-ray radiation (see Figure 1). Higher energy x-rays in the 50 to 100 keV range will be needed. 50-keV x-rays could be produced by nanosecond laser pulses if sufficient laser pulse energy is used. Unfortunately the scaling with pulse energy is very unfavorable. Some concepts for thermal x-ray backlighting call for use of up to 60 NIF beams illuminating one gas bag to produce one backlighter beam. On the other hand the scaling of x-ray energy and flux from high intensity lasers is much more favorable. In this case the laser light is converted with high efficiency to fast, forwardly directed electrons. These electrons are not in thermal equilibrium with the underlying plasma and

UCRL-JRNL-204814

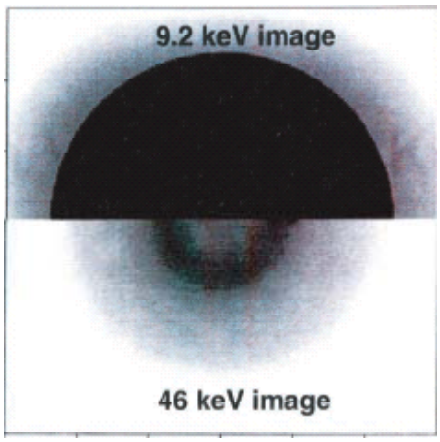

Figure 1. *Simulated radiograph of a NIF-like target with low and high energy x-rays corresponding to traditional thermal x-ray backlighting and HEPW driven x-ray backlighting respectively.*

can efficiently ionize inner shell electrons in the target material. The inner shell vacancies in turn lead to emission of x-ray line radiation. Significant Bremsstrahlung radiation is also generated by interaction of the fast electrons with the target material. In principle one 5-kJ class, picosecond laser pulse focused to relativistic intensities (~10^{18} W/cm^2) can in principle create enough k-alpha x-rays to accomplish the same high signal-to-noise radiography of a NIF-scale target that would require 10's of long pulse NIF beams.

In the Nova PW experimental campaign, it was found that fast electrons created by focused petawatt beams are able to efficiently produce beams of highly collimated, energetic protons. Proton radiography with HEPW laser-generated proton beams at energies up to 50 MeV is thus a feasible concept. Such radiography slightly lower energy has been shown to have micron-scale spatial resolution. In addition, the charge of the proton allows sensitivity to electric and magnetic fields otherwise not possible with x-ray radiography.

The high efficiency of conversion of HEPW laser energy to energy in a collimated proton beam opens up a new kind of isochoric heating in which the heating source is a proton-beam which is not connected to the heated object. This potentially allows a precisely fabricated object to be homogeneously heated by protons in a controlled fashion for equation or state and opacity studies. The range of accessible temperature is enhanced significantly by ballistic focusing of the protons from a concave surface, a process first demonstrated at the JanUSP laser at LLNL. [4]

The fast ignitor concept for inertial confinement fusion calls for the use of short pulse laser energy via energetic electrons or protons to heat compressed DT target. Recent integrated fast ignitor experiments at the Gekko laser facility at the Institute for Laser Engineering in Osaka, Japan have dramatically illustrated the potential of this concept. [5] In the Osaka experiments up to 1000 times more thermal neutrons have been produced from a short pulse heated compressed target. While compressed densities were insufficient to ignite the target, the Osaka work has established an important baseline with respect to coupling efficiency of short pulse laser light into fast electrons. Working backwards from the measured neutron yields suggests that ~20% coupling of laser light into fast electrons can be accomplished in a cone-focused, fast ignitor target arrangement. This coupling efficiency would suggest that full-scale, high-yield, fast ignition will require on the order of 100 kJ of short pulse laser light, or more than 2 orders of magnitude of energy beyond the present state of the art for high energy, short pulse laser systems.

II. HEPW Technology on NIF-like beam lines

High energy petawatt pulse production on NIF can be accomplished by adaptation of the chirped pulse amplification (CPA) technique to long-pulse NIF beam lines. In the CPA technique, a low-energy, wide-bandwidth, seed-pulse is passed through positive-dispersion delay line. This produces a long duration, positively chirped (red frequencies leading blue) pulse which is then amplified in the solid state amplifiers in much the same way as a narrow-bandwidth long pulse would be. In this way, pulse fluences approaching the saturation fluence of the gain media can be obtained without the onset of intensity dependent damage. After amplification, the high-energy, chirped pulse is passed through a negative-dispersion delay consisting of a pair or pairs of parallel diffraction gratings. This action removes the temporal chirp on the pulse and produces a high-energy, short-duration laser pulse. The peak power increase that may be obtained with the CPA technique is approximately given by the ratio to which the pulse is stretched and recompressed, typically on the order of 1000 to 10,000.

III. Dielectric Grating Design and Test

While the CPA technique is a highly effective method for eliminating short-pulse, intensity-dependent damage of the amplifier components, it does not eliminate short-pulse, final optic damage. The final optics in the CPA system, i.e. the last grating of the pulse compressor and the down-stream, beam-turning and focusing optics see both a high energy and short pulse duration and are thus potentially subject to intensity-dependent damage. Scaling of final optic aperture has been the traditional method of circumventing this problem. The 500-J Nova Petawatt for instance was enabled by development at LLNL of meter-scale, gold-coated, diffraction grating technology. Continued scaling of gold-grating technology

to produce HEPW pulses is, however, impractical. Doing so would require optical apertures in excess of 10-square-meters.

For higher fluences, a more promising solution is an all-dielectric grating. The type of grating is shown in Figure 2. These gratings can have a damage threshold nearly ten times that of gold gratings.

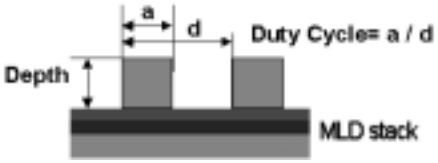

Figure 2 Schematic of MLD grating.

The theoretical limitation on the damage threshold of an MLD grating exposed to a short pulse results from the damage thresholds of the grating materials in combination with the field distribution in the grating.[6] The measured damage threshold may in addition be affected by such factors as 1) processing methods, e.g. removal of photoresist, 2) deviations between design parameters and manufactured grating, and 3) defects in the grating or multilayer stack. The MLD grating development at LLNL addresses all of these issues.

The grating design must satisfy several constraints. The grating must have high dispersion to limit the length of the compressor. The grating size is limited to about 1-m in our facility. This, along with the angle of incidence, determines the maximum beam size. The damage threshold is also a function of the incidence angle as discussed below. The grating profile and stack must have a high diffraction efficiency into the –1 order. The design must be manufacturable, a constraint that includes the requirement that the performance of any design must be relatively stable to small variations of its parameters.

The grating parameters that can be adjusted are the groove density, depth, shape and duty cycle, the latter being defined in Figure 2. The multilayer stack design is also critical to performance. The stack increases the efficiency and also influences the field distribution and therefore the damage threshold.

The grating and MLD stack are modeled using the code "LAMBDA" designed by Lifeng Li and based on a modal analysis which has been documented elsewhere.[7] This model is well suited to the rectangular grooves and TE polarization of interest here. A commercial code, TFCALC, is also used in MLD stack optimization.

The starting point of the design is a 1740-l/mm grating with an incidence angle of 61° (near Littrow). With a groove height of 620-nm and a duty cycle of 0.28, the predicted efficiency is >99%. The MLD stack consists of 20 layers of alternating Ta_2O_5 and Al_2O_3. Figure 3 shows the variation of diffraction efficiency with duty cycle and groove depth. High efficiency is maintained over a large variation of these parameters.

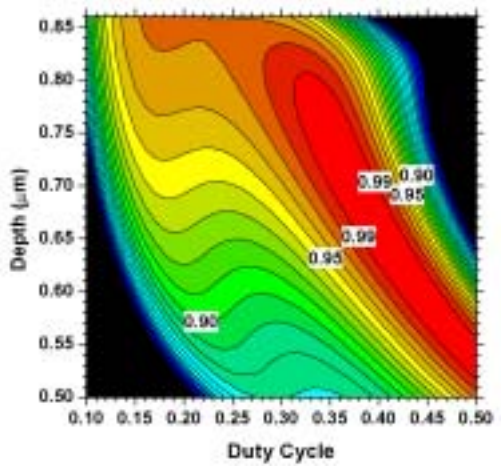

Fig. 3 The efficiency of the grating is above 95% over a wide range of depth and duty cycle variations.

The theoretical limit of the damage threshold occurs when the field in the dielectric materials of the grating exceeds the damage threshold of the material. Figure 4 shows contours of the magnitude of the field in units of the input field magnitude. The maximum field enhancement of 2.3 occurs a few hundred nanometers above the grating surface. The largest field enhancement in the grating materials occurs on the edge of the groove and is about 1.09 times the input field. The damage threshold of this grating then would be about 19% lower than that of the grating material, SiO_2.

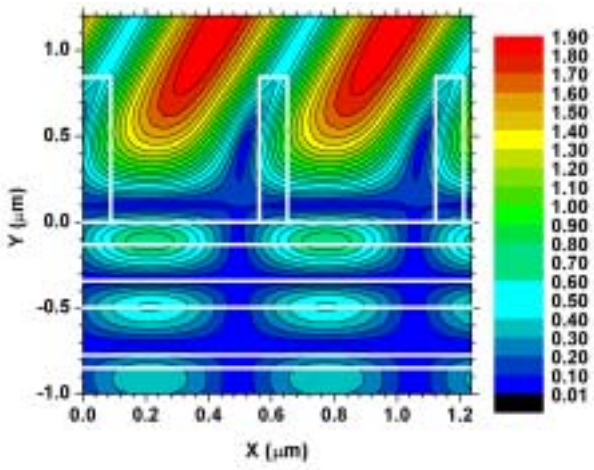

Fig. 4 Field distribution in one period of a 1780 l/mm grating and the top layers of the MLD stack.

Several parameters were varied in order to optimize the damage threshold. A small duty cycle gives a lower electric field enhancement with only a small decrease of efficiency. Angled grooves were found to have little effect.

The damage threshold can be significantly reduced by increasing the incidence angle. Figure 5 shows the field enhancement and efficiency of a 1780-l/mm grating. The field enhancement scales approximately as the illuminated area of the grating or the inverse of the cosine of the incidence angle.

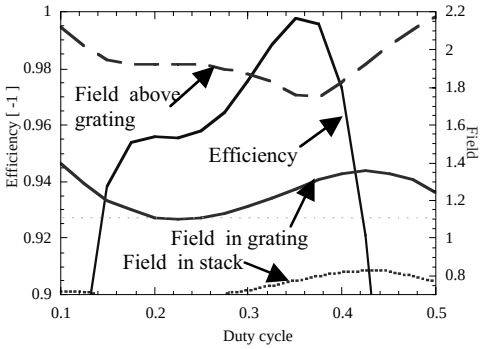

Fig. 5 Efficiency and field enhancement for a 1780-l/mm grating with a groove depth of 650nm and an incidence angle of 76.7°.

Verification of the model predictions for damage threshold requires a test facility with the capability of fully characterizing the temporal and spatial properties of the test beam. We have recently activated a dedicated facility to test subscale (50mm diameter) gratings.

The Precision Damage-Test Facility (PDTF) consists of three main subsystems, the laser source, the diagnostics and the damage-test table. The initial pulse for the laser source is generated by a commercial femtosecond laser, stretched with a grating pair and amplified to about 50mJ in an optical parametric chirped-pulse amplifier (OPCPA). The output pulse can be compressed to ~250fs although for most of the tests here the pulse is only partially compressed to give the desired pulse width. The laser operates at 10 Hz with a pulse-to-pulse energy stability of ±2% (one standard deviation).

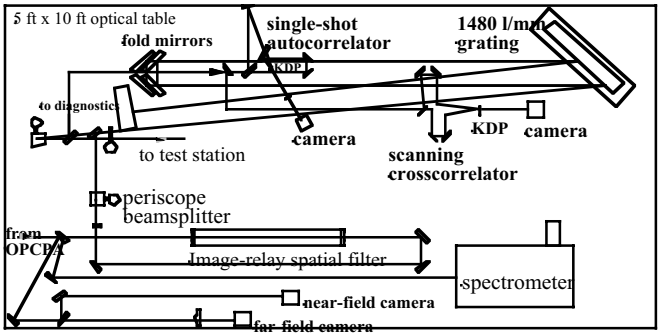

Fig. 6 Layout of diagnostics table of PDTF. The beams in the region of the compressor are at several different levels. The two passes of the main beam and the diagnostic beam are on four different levels about 30 cm above the table. The cross correlator and autocorrelator are about 6 cm above the table.

The compressor/diagnostics table is shown in figure 6. Before compression 4% of the output is split from the OPCPA for a diagnostic beam. The main output beam from the OPCPA is compressed by a 2-pass, folded compressor. The compressor length is adjusted to not fully compensate the dispersion of the pulse stretcher in order to generate the desired pulse duration for the damage test, typically 10ps. The diagnostic beam is injected into a pulse compressor which uses the same grating but a different set of fold mirrors whose distance from the grating can be independently set. The distance of this second set of fold mirrors is set to compress the diagnostic beam to its minimum pulse duration of about 0.25ps. The fully compressed diagnostic beam is mixed with the test beam in a 50-μm thick BBO crystal to form a second-order scanning cross correlator. Since the fully compressed pulse is much shorter than the test beam, the cross correlator gives the temporal profile of the test beam without the ambiguities of an autocorrelator. The disadvantage of the cross correlator is that it averages over many pulses.

Either the test beam or the diagnostic beam can be directed into a single-shot autocorrelator. This is used both to monitor the pulse-to-pulse stability of the temporal profile and to determine the pulse duration of the fully compressed diagnostic pulse. The spectrum of the laser is monitored and the measured spectrum is used to deconvolve the autocorrelation trace. The near field and far field spatial profiles of the laser are also monitored. These are primarily used for laser diagnostics. The test beam spatial profile at the sample plane is monitored on the damage-test table discussed below.

The layout of the damage-test table is shown in Figure 7. The ~1cm diameter beam from the compressor is focused onto the sample with a 2m focal length lens. A half-wave plate rotates the polarization so all measurements are done using TE polarization. The energy on the sample is monitored with a pyroelectric joulemeter that samples the beam through a partially reflecting mirror. This energy is calibrated using another energy

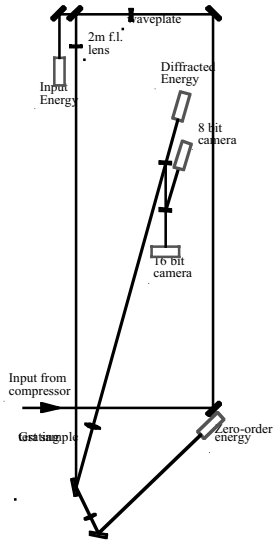

Fig. 7 Layout of damage-test table

meter placed in front of the test sample. Two other joulemeters measure the diffracted –1 order and the zero-order reflection.

The spatial profile of the beam on the sample is imaged onto both a 16-bit camera and an 8-bit camera. The 16-bit camera is used primarily to accurately measure the profile and the energy in the spatial wings of the beam. These measurements are taken prior to the damage measurement with a flat, fused silica sample at near normal incidence replacing the grating. The 8-bit camera is used primarily to monitor the diffracted beam from the grating on each shot. A typical beam profile at the sample is shown in figure 8.

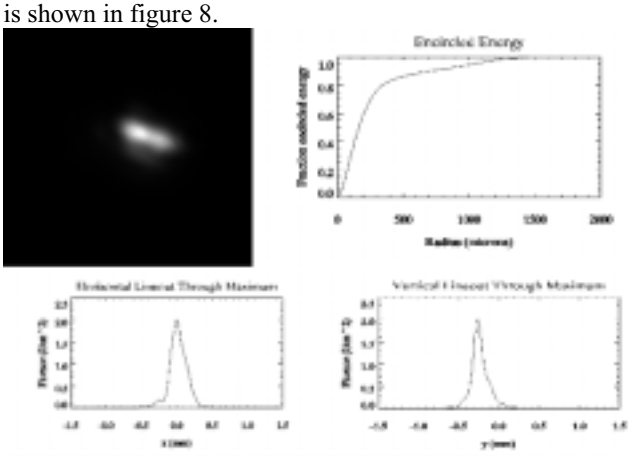

Fig. 8. a) 16-bit equivalent plane image of focal spot on sample. b) Encircled energy as a function of beam radius. c) and d) are spatial lineouts of the image in a).

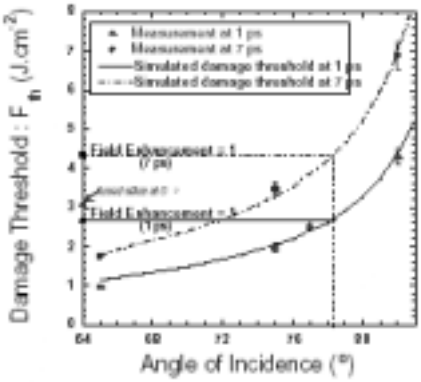

Fig. 9 – Damage threshold vs angle of incidence for an MLD grating for two pulse durations. Solid and dash lines are fits of experimental data with field-enhacement simulations based on the grating design. Damage threshold at normal incidence is given in comparison to the point where field-enhancement is equal to 1.

The dependence of damage threshold on incident angle is particularly important to the design of several high-energy petawatt systems planned or under development at LLNL. The verification of the model prediction of the angular dependence was the first investigation conducted. The results are shown in Figure 9.

This grating had a groove density of 1800 l/mm. This early data was taken with a slightly different setup, the primary difference being the lack of a cross correlator to verify pulse duration. Nevertheless, the measurements showed an excellent agreement between the model and the experimental results.

A large number of small scale grating samples have now been fabricated at LLNL and tested with the PDTF. To date, most of our tests have focused on gratings with a groove density of 1780 l/mm used at an angle of 76.5°. The best performing gratings of this type to date have exhibited a 'ramped' damage threshold (R:1) of up to 4.5 J/cm^2 at a 10 ps pulse duration Ramped damage studies "condition" the part as it is tested. The area illuminated by the test beam is not changed from shot to shot but the fluence at the illuminated position is slowly ramped from a low value until visible damage is observed with a long focal length microscope. Unconditioned, N:1 damage thresholds are lower but the magnitude of deviation from ramped values is part dependent. To date the best unconditioned N:1 damage threshold observed is 3.6 J/cm^2. of The best ramped damage results closely match the maximum theoretical damage threshold for the structure based on the predicted field enhancements of groove structure and the measured damage threshold of bare fused silica. We believe these are the highest damage threshold gratings of their type yet fabricated.

IV. Meter-scale MLD grating fabrication technology

Extensive efforts are underway at LLNL to develop the new tools and metrology required for extension of MLD grating fabrication from the 10's of cm to the meter-scale. In 2000, LLNL fabricated an MLD grating 355 x 150 mm in aperture that exhibited >99% diffraction efficiency for 1030 nm light at 63° incidence angle, that was used for a high-average power 50W short pulse machining laser [8]. In 2002, Jobin-Yvon-Horiba delivered high-peak power MLD gratings at 420x210 mm aperture to France's LULI laser.[9] HEPW pulse generation on the NIF laser will require either gratings of significantly larger aperture, or precision phasing of multiple gratings by a tiling approach[10] or both. The present baseline for HEPW pulse generation on NIF calls for tiling of two 91 cm MLD grating per grating aperture. Gratings of this size are more than a 100% larger than presently available commercially.

LLNL's grating manufacturing capability includes meter-scale holographic exposure and wet-processing tooling originally developed for the Nova Petawatt laser project. This tooling may be applied to meter-scale MLD grating fabrication. MLD grating fabrication however requires an additional etching step. Our ability to etch high-aspect ratio grating structures into hard dielectrics has been limited in the past. The recent commercial

development of linear RF powered ion sources for large area processing has opened up the possibility of etching processes based on linear tooling, a fundamental departure from the radially symmetric filament-based ion sources and planetary substrate motion of past devices. Such tools have the potential to provide uniform etching over large areas in compact geometries.

In 2002, we procured a prototype linear ion source from Veeco Ion Tech Inc., and built a custom-etching tool around it. This source is powered by 13.56 MHz RF at 2kW and produces a collimated ion beam 1.1 m long and 6 cm wide. Three stainless steel vacuum chambers from LLNL's mothballed Atomic Vapor Isotope Separation Facility, each 1.8-m x 1.5-m x 0.6-m (LxHxW) were joined to form one continuous chamber. The ion source was mounted vertically into a modified door of the center chamber, and a linear motion track was mounted along the floor to translate the substrate back and forth across the beam. A photograph of the installed tool is shown in Figure 10. The chamber is capable of $8x10^{-7}$ mmHg vacuum during pumpdown, and is plumbed for three gases, argon, oxygen and a freon compound for fluorine-based reactive chemistry for enhanced etching selectivity of oxide to mask material

Figure 10. Photograph of the ion-beam etcher. Ion source and substrate linear motion track in foreground awaiting installation.

The uniformity of the etched pattern is related to the uniformity of the ion beam, which provides reactive gases and energetic ions that impinge upon the substrate and remove material. The beam uniformity over the length of the source varies mainly because of non-uniformity in the RF power emission. This can be improved by optimal distribution of the gas flow rates over the length of the source, adjustment of the total system pressure, and by placement of partial grounding plates to attenuate the RF power locally along the length of the source.We built a Faraday cup current probe consisting of a stainless steel housing with a slotted aperture 20 cm wide by 0.75 cm high to allow the ion beam to impinge upon the carbon electrode mounted inside. This electrode is electrically isolated from the grounded housing and connected electrically to the beam control module, which applies a bias voltage and displays the current measured. All materials in the probe assembly are vacuum compatible and bake-able. The probe is mounted on a computer-controlled stage that provides vertical motion to scan the probe in the ion beam. The stage and probe are in turn mounted onto the substrate transport system, which allows positioning the probe laterally.

A number of experiments were performed varying the gas pressure and distribution, RF attenuator position, and acceleration and beam voltages, with the figure of merit being the RMS uniformity vertically over an 80-cm beam height. The ion current uniformity as a function of the beam height for the empirically-determined optimum parameter set is shown in Figure 11.

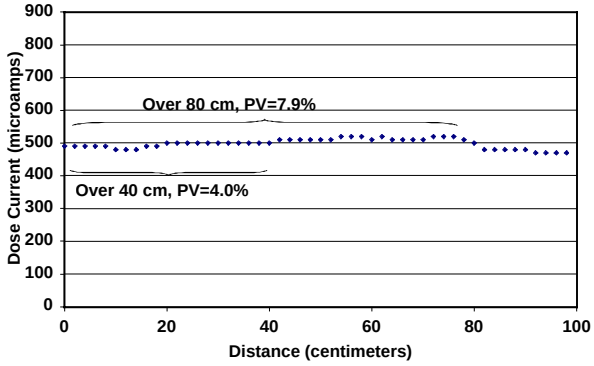

Figure 11: Ion current as function of vertical beam position for optimal conditions.

An 81-cm round window glass substrate was coated on site with approximately 300 nm of Ta_2O_5 and etched according to the above recipe, as a test of uniformity at large scale. Window glass was used to reduce costs, and Ta_2O_5 was chosen because it etches with the same

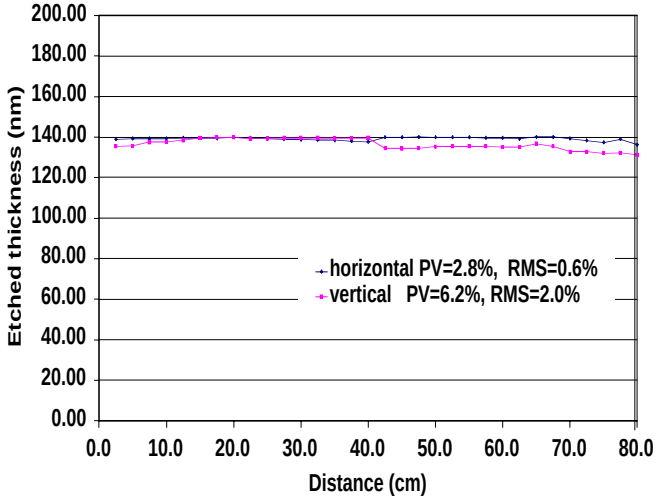

Figure 12. Ta2O5 film thickness removed on vertical and horizontal lineouts over 81 cm round optic.

chemistry as SiO_2 and the high index contrast between it and the window glass allows for inexpensive and fast interferometric measurements of the film thickness. The thickness of the Ta_2O_5 layer was measured at 2.5 cm intervals along the x and y axes of the substrate at its midpoint, before and after the etch run. The run was planned to remove approximately half the deposited film. The difference in the film thickness, representing the amount of etched material, is plotted in Figure 12. Horizontal etch depth nonuniformity is less than 3% absolute over 80 cm. The vertical nonuniformity of ~6% absolute agrees well with the vertical distribution of the ion current plotted in Figure 4. According to existing HEPW grating designs, a 6% variation in etch depth will not affect diffraction efficiency. However, since we do a slight overetch and employ an etch-stop layer with a selectivity of >10:1, the variation in etched depth with this tool at these conditions on a real grating would not be measurable.

Initial etching experiments on witness multilayer dielectric gratings have begun. Figure 13 shows a scanning electron micrograph of a 1740 line/mm MLD grating etched into a 700 nm thick SiO_2 top layer. Based on current removal rates, a grating 80 cm in long aperture could be transfer-etched to completion in approximately 9 hours under these conditions. Experiments to determine the effect of ion beam focus on the shape of the etched profiles are ongoing.

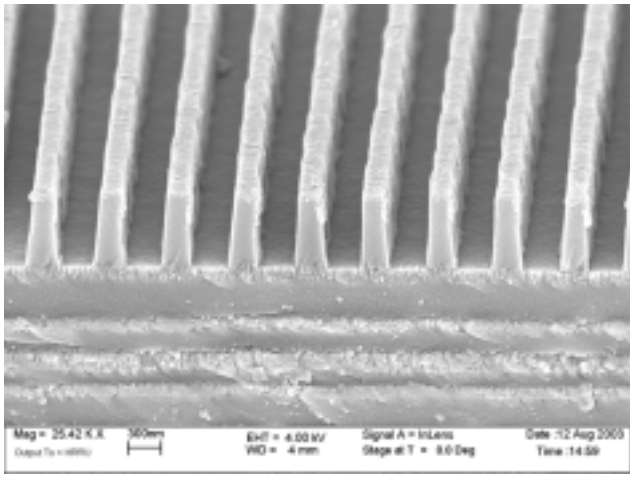

Figure 13. Scanning electron micrograph of 1740 line/mm witness multilayer dielectric grating etched in the large ion-beam etcher.

Recently a 40-cm x 80-cm blank (NIF polarizer) was coated at the Laboratory for Laser Energetics with an appropriate MLD grating coating and has been fabricated at LLNL to the approximate specifications for a NIF HEPW grating. This part is presently the world's largest, optical quality MLD grating (see Figure 14)

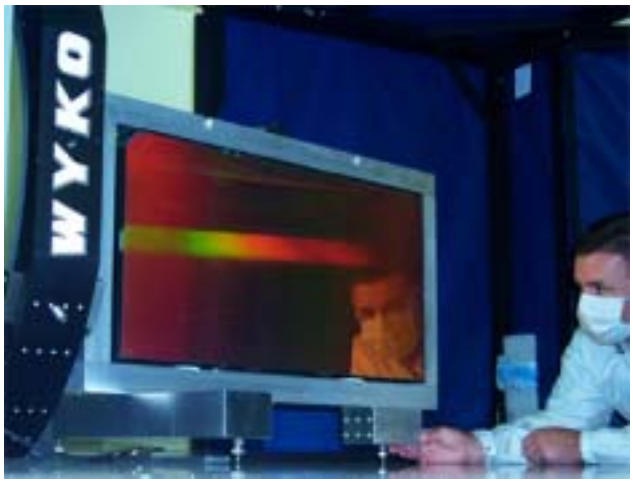

Figure 14. The world's first 80 cm scale, optical quality MLD grating fabricated at LLNL.

V. Fiber Front End

In addition to the fundamental final optics challenge, HEPW pulse production on NIF will be constrained in several instances by the architecture of the existing NIF hardware and facility. In order to be compatible with the existing layout and operating procedures an all-fiber front end is being developed. This effort seeks to create a system similar to the successfully deployed NIF front end laser architecture, which includes a fiber laser master oscillator, fiber amplifier chain and fiber transport to the NIF amplifier bay. Optical fiber technology offers many benefits for front ends for high-energy short pulse laser systems. These benefits include packaging for turn-key, robust, environmentally stable and low maintenance operation. Furthermore, some technology, such as chirped fiber Bragg gratings offer unique features not available in their bulk optic counterparts.

The front-end consists of an all-fiber mode-locked master oscillator, an electro-optic modulator (EOM) for pulse selection and amplified spontaneous emission control, a chirped fiber Bragg grating for pulse stretching (CFBG), a fiber pre-amplifier, a pulse width fail safe, transport fiber to take the pulses to the main amplifier bay and a final, specially-designed, high energy fiber amplifier.

Mode-locked fiber lasers have been demonstrated in the literature [11, 12, 13] with exceptional timing and energy stability as well as extremely broad bandwidths.

We have constructed similar devices from Yb-doped fiber at LLNL suited for our system needs.

To stretch the pulse prior to amplification we use a specially designed chirped fiber Bragg grating (CFBG). The CFBG is a chirped grating written into the core of an optical fiber such that the group delay as a function of wavelength is opposite in sign but equal in magnitude to that of the remaining laser chain plus pulse compressor. With existing technology it is possible to produce a stretched pulse of up to a few nano-seconds in duration. This technology is potentially very useful in short pulse laser front ends as one nominally has independent control over the group delay dispersion (GDD) and third order dispersion (TOD). Thus one can potentially compensate system dispersion issues up to second order. This will be especially important as it will allow precise compensation for the higher order phase distortion introduced by the greater than 80m of silica fiber to used to transport the short pulse oscillator output from the NIF master oscillator room (MOR) to the main amplifier chain.

Our design envisions flexibility surrounding the pulse energy and pulse width delivered to the target chamber. The final optics (gratings and focusing optics) have a pulse width dependent damage threshold. In order to avoid damage to the final optics the fiber includes a pulse width fail-safe. This device limits the final compressed pulse width for a given desired output energy. The device uses a pair of 1XN fiber optic switches to permit routing of the launched pulse through a selection of fiber lengths. The N individual fiber lengths will be selected to alter the pulse dispersion. In the case of the shortest length, the pulse will be fully compressed by the final compressor to its shortest pulse width. The remaining longer lengths of fiber will provide increasingly greater additional GDD and TOD to the pulse, mismatching it from the final compressor and resulting in a higher energy output but a recompressed pulse which is longer.

Presently NIF uses polarizing optical fiber for transport of long pulses from the master oscillator room (MOR) to the main amplifier bay. This fiber is essentially a polarization maintaining fiber with a depressed well index guiding structure[5]. This results in the creation of an operating window of typically 100nm bandwidth in which only one polarization state is guided. However application of this fiber to short pulses has a fundamental weakness. The dispersion of the fiber is strongly varying in the region of interest and includes large TOD components that are strong functions of the precise fiber that will be used and the geometry in which will be placed.

To combat this level of variability in the dispersion, a large mode area single mode optical fiber with active polarization control will be used. This will permit a predictable dispersion that is constant with time. A large mode area fiber will also permit maximization of the launched energy without the creation of B-integral issues. An appropriate large mode area fiber has been designed and ordered and tested for this application.

It has been shown through internal modeling[6] that gain narrowing in the Nd:glass amplifier chains will be the limiting factor in final pulse width delivered to the target. The high gain regenerative amplifier of the NIF pre-amplifier module (PAM) would induce most spectral narrowing. A high gain, broad-band fiber amplifier, would greatly improve the performance of the overall HEPW system. To be effective the fiber amplifier will need to produce mJ level, broadband output. This is an order of magnitude higher in pulse energy than typically available from commercial optical fiber amplifiers. We have recently developed and tested a new waveguide design called a large flattened mode (LFM).[14] This structure should be capable of producing chirped pulses with energies up to 20 mJ directly from the fiber. To date, the primary approach in scaling the pulse energy extractable from a rare earth doped optical fiber amplifier has been to scale the core size. So called large mode area (LMA) optical fibers permit increases in the extractable energy from the fiber core with decreasing the peak power in the core thus offsetting the impact of non-linear effects on the pulses which degrades the performance. The core size of a single mode optical fiber can be scaled to about 20μm diameter before one can no longer keep the fiber strictly single transverse mode. The core can be scaled as large as 50μm and schemes such as selective mode launch and bend induced attenuation of higher order modes can be employed to maintain good output beam quality. However, scaling beyond 50μm core size is problematic due to beam quality issues. At this core size, 1.2mJ has been extracted from an Yb^{3+} doped optical fiber amplifier, prior to the onset of limiting non-linear effects. Our LFM fiber design increases the output energy further by creating a fundamental guided mode, which is flat-toped rather than following the J_0 Bessel function shape found in a standard step index fiber design. This flat top shape is created by inclusion of a raised index ring surrounding the central core.[15]

In order to validate this fiber design, two fibers were specified, purchased and tested. The first was a 30-μm core, 0.06-NA, step-index, control fiber (Nufern) with a 400μm hexagonal cladding with a low index polymer coating (pump clad NA=0.37). The core was doped with Yb^{3+} such that there was an effective core absorption of 120dB/m at 977nm. A nearly identical fiber was also purchased from Nufern, but with the raised index ring that gives the LFM fiber its distinctive index profile. The inner core diameter of the LFM was 25.3μm and the outer core diameter was about 30-μm FWHM, the effective NA of the structure was approximately 0.06. The outer cladding and Yb^{3+} doping were the same as for the control fiber.

We then coupled 1.2-ns, 1075-nm, 10-Hz stretched mode-locked laser pulses into 9.1m of the control fiber

and 8.3m of the LFM fiber. The input energy coupled into the fiber cores was 15μJ. 977nm pump light from a 10W diode laser array was counter propagated through the fiber to pump the Yb^{3+} ions. The diode light was pulsed at 10Hz for 1ms timed to precede the arrival of the signal light. Both fibers produce roughly the same output energy as a function of pump diode current. The LFM fiber shows significantly less Raman energy build up as a function of diode current than the control fiber. This is in agreement with what we expected from the design. Greater than 0.6mJ output pulses have been obtained from the LFM amplifier with less than 5% of the energy in the Raman spectral band by utilizing pulses stretched to 3ns. With straightforward scaling of Yb^{3+} doping concentration to reduce the amplifier length, increasing the core size to 50μm and increasing the pump energy an optimized design could yield output pulses with greater than 10mJ of energy and virtually no degradation due to stimulated Raman scattering.

VI. Compact compressor arrangements

A more fundamental facility constraint for implementation of chirped pulse amplification on NIF is the availability of suitable floor space near the NIF target chamber for compression of the amplified chirped pulses. The Nova PW laser utilized a vacuum compressor chamber of order 12 meters in length. Multi-kilojoule, short pulse production on NIF will require longer stretched pulse duration. Nova PW style compressor technology would require of order 30 meters separation to compress NIF HEPW pulses. A vacuum chamber of this size would be difficult, if not impossible, to fit between the NIF target chamber wall and the 2 meter thick concrete wall located ~6 meters away. New, compact, high dispersion compressor designs are required for HEPW on NIF. Recently a novel mixed-grating, compact compressor design was developed at LLNL (see Figure 15). This design utilizes LLNL's advanced, high-dispersion, high-damage threshold MLD gratings and produces three times the dispersion of the Nova PW compressor while occupying a length of less than 5 meters. Compactness is achieved by using two sets of different groove density gratings for the compressor. The first set, which has slightly lower dispersion per meter of separation, accomplishes half of the pulse compression and produces a spatially chirped output. The second set, which has slightly higher dispersion per meter of separation, accomplishes the last half of the pulse compression and removes the spatial beam chirp. Because the grating sets have different separation, it is possible to produce an output beam which is parallel to the input beam but offset by a fixed amount. This allows the gratings to placed in close proximity to one another and greatly reduces the overall footprint of the compressor arrangement.

Figure 15. *Compact mixed grating pulse compressor. Gratings 1&2 are 1750 gr/mm while gratings 3&4 are 1780 gr/mm. The separations and angles of incidence have been adjusted so that the output has no spatial chirp.*

VII. Implementation and Conclusions

A concept for integrating a single HEPW beam line and later a quad of HEPW beams into NIF has been developed. This concept would allow implementation with minimal impact to the existing NIF architecture. NIF line replaceable units (LRUs) would be replaced with short pulse LRUs. Fiber-based, short pulse front-end components would be deployed in the NIF MOR and on an existing PAM. No modifications are required to the NIF amplifier chain and the beam is formatted to fit within the NIF baseline clear aperture of 40 x 40 cm^2. This allows the use of NIF mirrors and mounts and dramatically minimizes cost. The format will allow one quad of beams to be rapidly and precisely switched between long and short pulse operation thus not effecting ignition campaigns on NIF requiring all 192 beams. In the target bay, redirection of 1 to 4 beams of the quad into an optical pulse compressor will be accomplished with pick-off mirrors and will enable real-time conversion between HEPW and long pulse operation. The compact pulse compressor and final optics concept accommodates quad deployment by utilizing two compressor vacuum vessels, each of which contains optics for two beams of the quad. These vessels can accommodate multiple grating arrangements and will allow a phased deployment of short pulse capability. In the initial phase, the grating aperture will be limited to 40 x 90 cm and the input beam shape will be limited to 16 x 40 cm so as to not overfill this aperture. Future phases will utilize coherently tiled pairs of 40 x 90 cm gratings to accommodate the full NIF beam aperture. Following compression the beams will be directed to the NIF target chamber center via a presently unused, direct-drive, equatorial port and focused by a 90

degree, 9-m focal length, off-axis parabola. This system will allow generation of > 2 kJ of short pulse energy per beam line and generation of focal intensities at target chamber center > 5 x 10^{19} W/cm^2.

The energy and intensity of these pulses will be sufficient to meet the primary high-energy, x-ray radiographic needs of large-scale target experiments which are presently part of the planned first cluster NIF experimental campaigns.

VIII. References

1. D. Strickland and G. Mourou, "Compression of amplified chirped optical pulses," Opt. Commun. **56**, 219-221 (1985).
2. M. D. Perry, D. Pennington, B. C. Stuart, G. Tiethohl, J. A. Britten, C. Brown, S. Herman, B. Golick, M. Kartz, J. Miller, H. T. Powell, M. Vergino, and V. Yanovsky, "Petawatt laser pulses," Opt. Lett. **24**, 160-162 (1999).
3. J. D. Bonlie, F. Patterson, D. Price, B. White, and P. Springer, "Production of >10^{21} W/cm^2 from a large-aperture Ti:sapphire laser system," Appl. Phys. B **70**, 155-160 (2000).
4. P. K. Patel, A. J. Machinnon, M. H. Key, T. E. Cowan, M. E. Foord, M. Allen, D. F. Price, H. Ruhl, P. T. Springer and R. Stephens, "Isochoric Heating of Solid-Density Matter with an Ultrafast Proton Beam", Phys. Rev. Lett., 91, 2003
5. R. Kodama et al., "Fast Heating of Ultrahigh-Density Plasma as a Step Towards Laser Fusion Ignition", Nature, 412, 798 (2001)
6. R.D. Boyd, J.A. Britten, D. E. Decker, B. W. Shore, B. C. Stuart, M. D. Perry and Lifeng Li, "High-Efficiency Metallic Diffraction Gratings for Laser Applications," Appl.Opt. 34, 10 1697 (1995)
7. L. Li, "A Multilayer Modal Method for Diffraction Gratings of Arbitrary Profile, Depth, and Permittivity," JOSA A, 10, 12 2581 (1993)
8. J.A. Britten, S.J. Bryan, L.J. Summers, H.T. Nguyen, B.W. Shore, O. Lyngnes. 'Large aperture, high-efficiency multilayer dielectric reflection gratings.' *presented at the Conference on Lasers and Electro-Optics. Conference Edition (IEEE Cat. No.02CH37337). Opt. Soc. America. Part vol.2, 2002, pp.CPDB7-1-4 vol.2. Washington, DC, USAW*.
9. B. Touzet, 'Large gold and Multilayer Dielectric Gratings: a Review of Current Performances', *Workshop on Technological Bottlenecks in Compact High-Intensity Short Pulse Lasers, Paris France, OECD Global Science Forum, J.P. Chambaret, editor, April 1-4, 2003*
10. T.J. Kessler, J. Bunkenburg, H. Huang, A. Kozlov, and D.D. Meyerhofer, 'Demonstration of coherent addition of multiple gratings for high energy chirped-pulse-amplified lasers", Optics Letters, submitted (2000)
11. J.H.V. Price, L. Lefort, D.J. Richardson, G.J. Spuhler, R. Paschotta, U. Keller, C. p. J. Barty, A. Fry, J. Weston, CLEO 2001 paper CTuQ6
12. L. Lefort, A. Albert, V. Couderc, A. Barthelemy, IEEE Photonics Technology Letters, vol 14, pp 1674-1676, 2002
13. H. Lim, F. Ilday, F. Wise, ASSP 2003 paper PD5
14. J.W. Dawson, Z.M. Liao, I. Jovanovic, B. Wattellier, R. Beach, S.A. Payne, C. P. J. Barty CLEO 2003
15. A. K. Ghatak, I. C. Goyal, R. Jindal, "Design of waveguide refractive index profile to obtain flat modal field" SPIE Proceedings vol. 3666, pp. 40 (1998)

This work was performed under the auspices of the U. S. Department of Energy by Lawrence Livermore National Laboratory under Contract No. W-7405-Eng-48.